Theoretical Study of Mg^+-X and $[X-Mg-Y]^+$ Complexes Important in the Chemistry of Ionospheric Magnesium (X, Y = H_2O, CO_2, N_2, O_2, and O)

Richard J. Plowright,[†] Thomas J. McDonnell,[†] Timothy G. Wright,*[,†] and John M. C. Plane[‡]

School of Chemistry, University of Nottingham, University Park, Nottingham NG7 2RD U.K., and School of Chemistry, University of Leeds, Leeds, LS2 9JT U.K.

Received: June 16, 2009; Revised Manuscript Received: July 7, 2009

Optimized geometries and vibrational frequencies were calculated for Mg^+-X and $[X-Mg-Y]^+$ complexes (X, Y = H_2O, N_2, CO_2, O_2, and O), required for understanding the chemistry of magnesium in the upper atmosphere. B3LYP optimizations were performed employing 6-311+G(2d,p) basis sets. In several cases a number of different orientations were investigated in order to determine the geometries of lowest energy, and in cases involving O and O_2, different spin states also had to be considered. In contrast to the corresponding Ca^+-containing complexes, the diligated Mg^+ ions have the two ligands approaching from the same side. In order to establish accurate energetics, up to RCCSD(T) single-point energy calculations were also employed, using quadruple-ζ basis sets. Accurate dissociation energies for the Mg^+-X and $[X-Mg-Y]^+$ species were derived and discussed. Comparison with available experimental results was made where possible.

1. Introduction

Up to an estimated 150 metric tons of interplanetary dust enters the Earth's atmosphere each day. Most of this dust ablates to provide a source of metallic atoms and ions between 70 and 120 km.[1] The chemistry of metals in the upper atmosphere has been linked with a number of interesting phenomena, such as the formation of sporadic metal layers, persistent meteor trails, and noctilucent clouds, and has been reviewed at regular intervals.[1−4] In addition, the extraterrestrial supply of metals has been postulated[5] as being a significant source for biosystems in remote environments where the aeolian supply is limited.

One of the major metals in the mesosphere and lower thermosphere (MLT) region, produced by the ablation of interplanetary particles, is magnesium. This deposition mechanism accounts for the addition of approximately 6 tons of magnesium per day,[6] forming a global layer of atomic Mg between 80 and 110 km in the Earth's atmosphere. Magnesium is also thought to be of importance in other atmospheres, such as Titan's.[7]

These meteoric particles ablate owing to frictional heating with ambient air, and the altitude at which the metals are present is correlated with their vaporization temperatures: more volatile elements are found at higher altitudes, while more refractory elements travel further before ablating.[8] It is this differential ablation process which accounts for the difference in the abundances of metallic species in chrondritic meteorites and in the MLT region.[9]

Sporadic metal layers, M_s, are thin layers (typically about 1 km wide) of metal atoms, M, which appear over a matter of minutes and can last for several hours, before rapidly disappearing.[10] M_s exist for a number of metals present in the MLT and were first observed for sodium atoms (Na_s).[11−14] These layers arise from the neutralization of sporadic E layers (E_s), which are comprised of mainly metal ions, with Mg^+ and Fe^+ being the dominant metallic species.[4]

Ablated Mg atoms can be ionized via hyperthermal collisions with atmospheric molecules. Furthermore, the plasma in the lower E-region is dominated by ambient NO^+ and O_2^+ ions which form Mg^+ through charge transfer reactions (reactions 1 and 2). The Mg^+ cation can also be formed through photoionization (reaction 3).

$$Mg + NO^+ \rightarrow Mg^+ + NO \quad (1)$$

$$Mg + O_2^+ \rightarrow Mg^+ + O_2 \quad (2)$$

$$Mg + h\nu \rightarrow Mg^+ + e^- \quad (3)$$

The present work details a theoretical study of the ion−molecule chemistry of magnesium, which is essential in developing an understanding of the coupling of Mg and Mg^+ in the MLT, and enables further insight into the interesting phenomenon of sporadic magnesium layers (Mg_s) which develop in this region of the atmosphere.

This neutralization of Mg^+ can occur directly through radiative recombination with electrons (reaction 4), although this mechanism has been found to be very inefficient.[15] It is more likely that Mg^+ will form molecular complex ions via reactions with O_3 (reaction 5) or via association reactions with X (=N_2, O_2, CO_2, or H_2O) in the presence of a third body, M (reaction 6). These new species can undergo ligand switching (reactions 7a, 7b), which would proceed via an energized diligand intermediate complex $(X-Mg^+-Y)^*$, which can decompose to yield either $Mg^+-X + Y$ or $X + Mg^+-Y$ (reaction 7a), or, if the pressure is high enough, be stabilized by a third body M (reaction 7b). Stabilization of the diligand intermediate by M may also occur if X = Y (reaction 8), and this can initiate the buildup of a cluster. In particular, for the case X = H_2O, ion hydrates have been postulated as ice nuclei for noctilucent clouds.[16] An Mg_s layer can then arise from

[†] University of Nottingham.
[‡] University of Leeds.

10.1021/jp905642h CCC: $40.75
Published on Web 07/28/2009

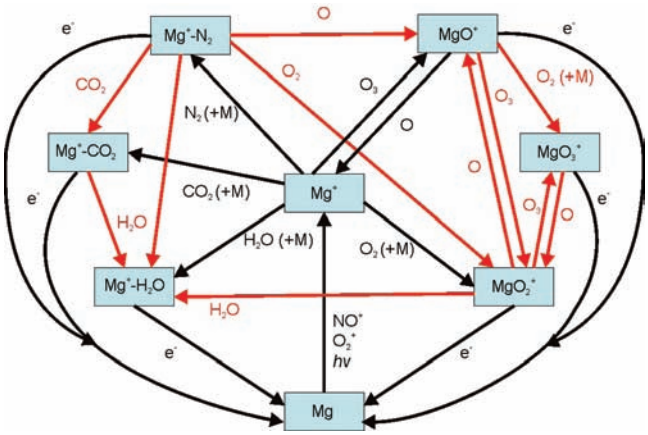

Figure 1. Schematic diagram of the ion−molecule chemistry of magnesium in the mesosphere−lower thermosphere.

dissociative recombination of these molecular ions with electrons (reaction 9). A schematic diagram of this chemistry is shown in Figure 1.

$$Mg^+ + e^- \rightarrow Mg + h\nu \quad (4)$$

$$Mg^+ + O_3 \rightarrow MgO^+ + O_2 \quad (5)$$

$$Mg^+ + X \xrightarrow{M} Mg^+-X + M \quad (6)$$

$$Mg^+-X + Y \rightarrow X-Mg^+-Y^* \rightarrow Mg^+-Y + X \quad (7a)$$

$$\rightarrow X-Mg^+-Y^* \xrightarrow{M} X-Mg^+-Y \quad (7b)$$

$$Mg^+-X + X \xrightarrow{M} X-Mg^+-X \quad (8)$$

$$Mg^+-Y + e^- \rightarrow Mg + Y \quad (9)$$

This proposed ion−molecule chemistry is based on our previous work on the sporadic layer chemistry of Ca,[17] Na,[14,18] and K.[19] In those studies, ab initio calculations were employed, initially using the B3LYP method with a 6-311+G(2d,p) basis set. These geometries were then compared to MP2 and QCISD[19] ones obtained with the same basis set. The geometries established from these methods were used as input data to allow single-point energies at the RCCSD(T)/aug-cc-pVQZ level of theory to be obtained more reliably. These spectroscopic constants provided data for the application of Rice−Ramsperger−Kassell−Marcus (RRKM) theory, which has been used both to estimate rate coefficients for atmospheric modeling[14,19] and to extrapolate laboratory measurements of rate coefficients to the conditions of the MLT.[20]

Atomic Mg^+ ions have been detected in the mesosphere and lower thermosphere by rocket-borne mass spectrometry,[21−23] by photometric observations performed by rockets[24] and satellites,[25] and more recently by the satellite-borne SCIAMACHY spectrometer measuring the dayglow in the limb.[8] Detection of neutral atomic Mg in the upper atmosphere is limited to satellite-borne experiments.[8] This is due to the fact that the $Mg(3^1P_1-3^1S_0)$ transition at 285.2 nm is overlapped by the Huggins and Hartley bands of ozone,[6] making ground-based observations, by a technique such as LIDAR, impossible owing to the amount of ozone in the stratosphere.

The difficulty of accessing the MLT region directly has led to chemical modeling of this region proving to be a powerful tool in the armory of the atmospheric chemist, with quantum chemical calculations linked to thermodynamics and kinetics; in the most useful cases, these are convolved with atmospheric parameters (partial pressures, electron densities, and temperatures) to yield predicted concentration profiles, which can be compared with observations (both in the Earth's atmosphere[14] and in the laboratory[4]). As well as our work on Na,[18] K,[19] and Ca,[17] there have also been studies on Al,[26,27] Mg,[27−30] and Si.[28] A recent study[30] on magnesium has termed the $MgOH^+$ ion "pivotal", and indeed this ion was considered in early work.[31] However, the importance of $MgOH^+$ seems unlikely given the relatively low concentration of H_2O_2, which is required to form it through reaction with Mg^+. $[H_2O_2]$ is predicted to be at least 2 orders of magnitude less than $[O_3]$ above 70 km,[32] so that either reaction 8 or recombination with O_2 will be the dominant reactions of Mg^+ in the MLT. In the present work, we perform a set of calculations similar to those we reported recently[17] for Ca sporadic layers.

2. Calculational Details

Calculations were carried out on Mg^+-X and $[X-Mg-Y]^+$ intermediate ionic complexes using the Gaussian 03 suite of programs,[33] in order to obtain accurate binding energies, harmonic vibrational frequencies, and rotational constants. In previous investigations on similar systems[17−19] little difference was observed between the optimized geometries obtained at the B3LYP, MP2, and QCISD levels of theory. Owing to time and cost constraints, subsequent higher-level single-point calculations were performed at geometries obtained using the B3LYP method. We therefore follow a similar procedure in the present work, but we have only performed geometry optimization calculations at the B3LYP level with a Pople 6-311+G(2d,p) triple-ζ basis set level. The B3LYP energies were used to calculate binding energies, D_e; we also obtained D_0 values by applying zero-point vibrational energy (ZPVE) corrections. In addition, we performed UCCSD(T)/aug-cc-pVQZ single-point calculations at the B3LYP-optimized geometries using Gaussian, where only the valence electrons were correlated. Subsequent RCCSD(T) single-point calculations employed Molpro,[34] with the standard aug-cc-pVQZ basis sets being used for first-row elements, while for Mg^+ the aug-cc-pCVQZ basis set was employed. In the RCCSD(T) calculations, only the Mg, N, C, and O 1s orbitals were kept frozen, which is why a basis set for Mg^+ was selected which includes "tight" functions to describe the core−valence correlation. In both sets of CCSD(T) calculation, the B3LYP vibrational energies were employed to correct D_e to D_0 values. The complete basis set method (CBS-Q)[35] is a relatively cheap method which often produces surprisingly good energetics. We have therefore included CBS-Q bond energies for comparison with the high-level RCCSD(T) results.

3. Results and Discussion

3.1. Ab initio Calculations on Mg^+-X Complexes. ***3.1.1. Mg^+-H_2O.*** There have been a number of photodissociation experiments reported on the Mg^+-H_2O complex (and higher complexes) and its fully deuterated isotopomer.[36−44] The

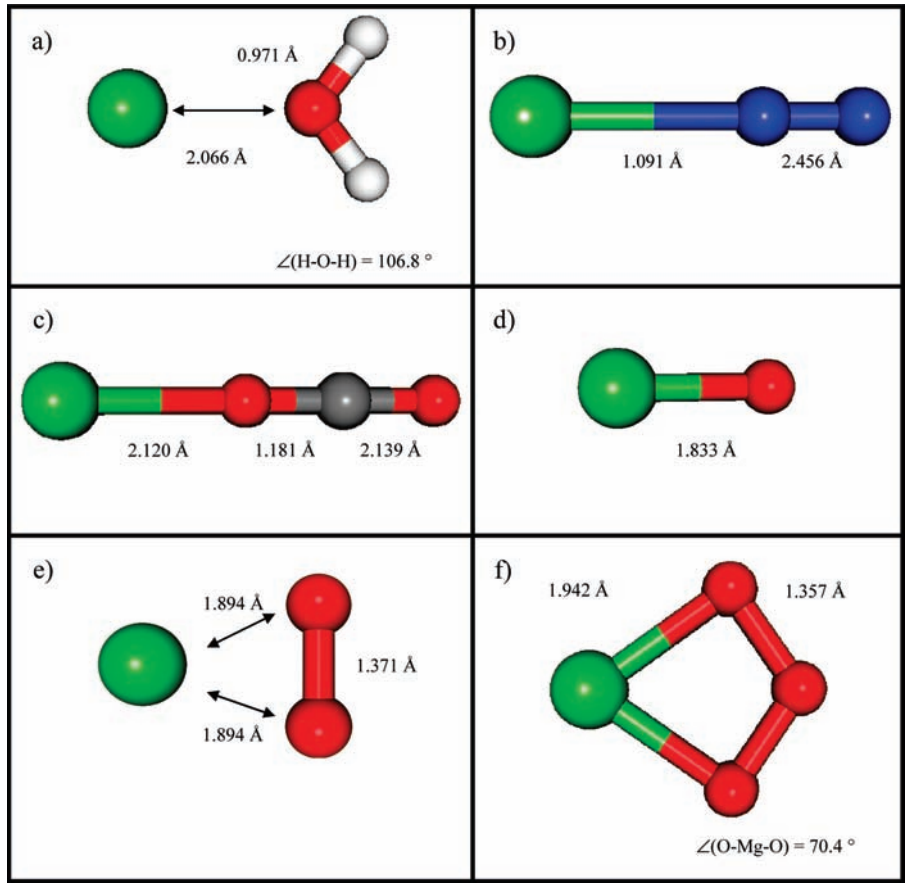

Figure 2. B3LYP/6-311+G(2d,p) optimized geometries of Mg^+-X complexes. Bond lengths in angstroms and bond angles in degrees. See text for details.

TABLE 1: Harmonic Vibrational Frequencies and Rotational Constants of Mg^+-X Complexes Obtained at B3LYP/6-311+G(2d,p) Level of Theory[a]

X	state	total energy (E_h)	vibrational frequencies (cm^{-1})	rotational constants (GHz)
CO_2	$^2\Sigma^+$	−388.484 007	61 (π), 243 (σ), 641 (π), 1364 (σ), 2433 (σ)	0.00, 2.40, 2.40
H_2O	$^2A_1$	−276.320 972	348 (b_1), 381 (a_1), 510 (b_2), 1660 (a_1), 3717 (a_1), 3795 (b_2)	412.82, 10.69, 10.42
			394 (a_1), 460 (b_1), 570 (b_2), 1798 (a_1), 4024 (a_1), 4105 (b_2)[b]	
N_2	$^2\Sigma^+$	−309.384 456	130 (π), 164 (σ), 2443 (σ)	0.00, 4.03, 4.03
			150 (π), 178 (σ), 2424 (σ)[c]	
			148 (π), 174 (σ), 2390 (σ)[d]	
O_3	$^2B_1$	−425.403 527	261 (b_1), 446 (b_2), 476 (a_1), 766 (a_1), 872 (b_2), 1066 (a_1)	12.60, 8.35, 5.02
O	$^2\Pi$	−274.980 294	709 (σ)	0.00, 15.67, 15.67
			902[e]	
O_2	$^2A_2$	−350.204 815	524 (b_2), 656 (a_1), 1110 (a_1)	33.62, 11.83, 8.75

[a] Italicized values are from previous work: see the appropriate footnotes. [b] Reference 47, SCF values. [c] Reference 51, MRCI+Q values. [d] Reference 51, MCPF values [e] Reference 56, CISD value.

first of these studies yielded a very high D_0 value of 251 ± 20 kJ mol^{-1},[36] but later studies yielded 104 kJ mol^{-1} (see ref 37) and 102 kJ mol^{-1} (ref 38).

Our optimized geometry (Figure 2a) is very similar to those obtained by other workers; the vibrational frequencies and rotational constants are reported in Table 1. Our D_0 value using RCCSD(T) theory, 130.8 kJ mol^{-1}, for the $\tilde{X}^2A_1$ state is somewhat higher than the later experimental values (see Table 2), but is in excellent agreement with the B3LYP, UCCSD(T), and CBS-Q values (see Table 2). Other theoretical values have yielded 150 ± 20 kJ mol^{-1} (ref 45, also cited in ref 46) using the MCPF approach with fairly large basis sets, 130 kJ mol^{-1} using the CASSCF + MRCI approach,[47] 155 kJ mol^{-1} in ref 40 using the POLCI approach, and 160 kJ mol^{-1} using the MP4 approach.[43] All of these values are higher than the more recent spectroscopic values,[37,38] but are lower than the earlier one.[36] More recently, a value of 119 kJ mol^{-1} was obtained in MP2/6-311+G(2d,2p) calculations by Andersen et al.,[48] with values of 119.6 and 121.7 kJ mol^{-1} being reported by Dunbar and Petrie[49] using both CP-MP2(thaw) and the CP-dG2thaw single-point calculations, respectively, at the B3LYP/6-311+G** optimized geometry. Given the higher level of theory employed herein, and the agreement between our RCCSD(T), UCCSD(T), CBS-Q, and B3LYP values and other more recent values, it is likely that the theoretical binding energy value is the more reliable, and that the experimental value is in need of remeasurement.

It seems that there has only been one earlier report of vibrational frequencies, and these only at the Hartree−Fock level,[47] where the ordering of the lowest two vibrational frequencies is different from that obtained here (see Table 1). Again, experimental measurement of these quantities is desirable.

TABLE 2: Dissociation Energies (D_0 (D_e) in kJ mol^{-1}) for Mg^+-X Complexes (X = H_2O, CO_2, N_2, O, O_2, and O_3)

	species					
level of theory	Mg^+-H_2O	Mg^+-CO_2	Mg^+-N_2	Mg^+-O	Mg^+-O_3	Mg^+-O_2
B3LYP	131 (137)	62 (63)	28 (31)	208 (213)	269 (273)	51 (55)
CBS-Q	127	64	36	224	263	90
UCCSD(T)[a]	127	64	28	218	266	89
RCCSD(T)[b]	131 (137)	67 (69)	30 (33)	216 (220)	261 (265)	90 (94)
experimental	102[38]	62[53]		220 ± 15[36] $110 < D_0 < 300$[58] $110 < D_0 < 300$[60] 240 ± 10[61]		≤ 110[63]
previous theoretical	150[45]	66[54] 61[49]	41[51]	224[55] 228[57]	119[30]	98[62] 36[57]

[a] UCCSD(T) calculations performed with Gaussian. Only valence electrons were correlated. The aug-cc-pVQZ basis set was employed. [b] RCCSD(T) calculations performed with MOLPRO. Only the 1s orbitals of Mg, N, C, and O were frozen. The aug-cc-pCVQZ basis set was employed.

3.1.2. Mg^+-N_2. In line with our previous work on Ca^+-X[17] and electrostatic considerations,[39] the present calculations confirmed the expectation that N_2 prefers to bind end-on giving a linear $^2\Sigma^+$ state (see Figure 2b), a result which is in line with previous theoretical[50,51] results. Our RCCSD(T) value of 30.1 kJ mol^{-1} is close to our B3LYP and UCCSD(T) values (see Table 2). It is also in reasonable agreement with our CBS-Q calculation and the previous MRCI+Q value obtained by Maitre and Bauschlicher.[51] The derived D_0 value obtained in photodissociation experiments[52] was deemed unreliable therein, since the observed vibrational progression in the electronic spectrum was not thought to correspond to the $Mg^+\cdots N_2$ stretch. The vibrational frequencies are presented in Table 1, together with those obtained in ref 51 at both the MCPF and MRCI+Q levels of theory; good agreement is seen.

3.1.3. Mg^+-CO_2. As rationalized below, we only considered end-on bonding of Mg^+ with CO_2, yielding a $^2\Sigma^+$ state, with the calculated geometry being shown in Figure 2c—this was based on both our previous Ca^+ work[17] and electrostatic arguments.[39] The RCCSD(T) D_0 value (see Table 2) of 67.0 kJ mol^{-1} is in relatively good agreement with the value of 62 kJ mol^{-1}, indirectly derived from a (long) Birge−Sponer extrapolation to yield the dissociation energy for the observed excited $^2\Pi$ state by Willey et al. in photodissociation experiments.[53] There is a more recent value of 58 ± 6 kJ mol^{-1} obtained by Andersen et al.[48] using guided ion beams, which is slightly lower than the present value, although in agreement (within experimental error) with the spectroscopic value.

There is very good agreement between the different levels of theory employed herein (Table 2). A previous theoretical value of 66 kJ mol^{-1} by Sodupe et al.,[54] obtained at the MCPF level of theory with large basis sets, is also in excellent agreement with our RCCSD(T) value, and has a very similar geometry (see Figure 2). No vibrational frequencies were reported in ref 54 with which to compare our values listed in Table 1. A value of 54 kJ mol^{-1} obtained at the MP2/6-311+G(2d,2p) level of theory in ref 48 seems somewhat low. The most recent values appear to be those of Dunbar and Petrie[49] using both CP-MP2(thaw) and the CP-dG2thaw single-point calculations at the B3LYP/6-311+G** optimized geometry: the values of 53.9 and 60.7 kJ mol^{-1}, respectively, are both a little below those obtained here and those obtained in ref 54. It seems that this quantity is somewhat basis set dependent, but given the consistency between the present values and those of ref 54, the present RCCSD(T) is likely the most reliable, and the experimental values, and other theoretical ones, are likely slightly too low.

3.1.4. MgO^+. The ground state of Mg^+-O is $^2\Pi$, and may largely be described as $Mg^{2+}-O^-$, with the bond length obtained indicated in Figure 2d. Our RCCSD(T) binding energy of 216.2 kJ mol^{-1} is in very good agreement with the redetermined theoretical value[55] of 224 ± 6 kJ mol^{-1} (confirming the earlier value of 223 kJ mol^{-1})[56] from Bauschlicher et al., using both MCPF and CCSD(T) calculations, only freezing the 1s orbitals on all atoms, and employing augmented basis sets of quadruple- and quintuple-ζ quality. In addition, there is very good agreement with our UCCSD(T) and CBS-Q values (Table 2), and an earlier CBS-Q calculation of 227.7 kJ mol^{-1} from Jursic,[57] but the B3LYP value is slightly low.

In addition there are a number of experimental values. The earliest appears to be from the ion cyclotron resonance (ICR) studies of Kappes and Staley,[58] who obtained a bracketed value, $110 < D_0 < 170$ kJ mol^{-1}, based on the fact that they were unable to observe MgO^+ when reacting Mg^+ with N_2O, but observed it in the reaction with O_3. We have recently confirmed this experimental result, and show that the reaction $Mg^+ + N_2O$ is very slow because there is actually a barrier of around 47 kJ mol^{-1} on the potential energy surface.[59] Flowing afterglow studies reported by Rowe et al.[60] yielded a range of $106 < D_0 < 300$ kJ mol^{-1}, which is consistent with the theoretical values, albeit that the range is wide. Mass spectrometric experiments from Operti et al.[36] derived a value of $D_0 = 220 \pm 13$ kJ mol^{-1}, which is in excellent agreement with the derived theoretical values. A subsequent determination of 240 ± 10 kJ mol^{-1} from guided ion beam studies by Dalleska and Armentrout[61] on $Mg^+ + O_2$ was concluded as being slightly too high by Bauschlicher et al.,[55] a conclusion with which we concur.

3.1.5. MgO_2^+. Like N_2, it is possible for O_2 to bind either end-on or side-on, and in addition the complex can have an overall doublet or quartet multiplicity state. Our findings are in accordance with previous calculations[62] which indicate the O_2 binds side-on, giving rise to an $\tilde{X}^2A_2$ state—Figure 2e shows the geometry. This doublet state occurs as a result of charge transfer from the Mg^+ to the oxygen, effectively giving $Mg^{2+}O_2^-$, and is in line with previous conclusions[17] reached for CaO_2^+. Our RCCSD(T) calculated dissociation energy of $D_0 = 90$ kJ mol^{-1} (Table 2) is in very good agreement with a previously determined theoretical value of 97.5 kJ mol^{-1}, obtained using the MCPF approach and atomic natural orbitals,[62] and is also in line with photodissociation experiments,[63] which derived $D_0 \leq 110$ kJ mol^{-1}. Interestingly, the B3LYP value is very much lower than the RCCSD(T) one, but there is good agreement between RCCSD(T), UCCSD(T), and the present CBS-Q values. (Jursic[57] obtained a very low result of 35.6 kJ

mol^{-1} using the CBS-Q method, suggesting an error therein.) Our vibrational frequencies (Table 1) appear to be the only ones reported to date.

3.1.6. MgO_3^+. The optimized geometry of the of MgO_3^+ is of C_{2v} symmetry, $\tilde{X}^2B_1$ (see Figure 2f), and can again be described largely in terms of a charge transfer, yielding $Mg^{2+}-O_3^-$. The binding energy we obtain is $D_0 = 261$ kJ mol^{-1}, which is very similar to the B3LYP, UCCSD(T), and CBS-Q values. We note that there has been a previous report of the binding energy for MgO_3^+, yielding values of only 131.2 and 118.5 kJ mol^{-1} at the dG2thaw and CP-dG2thaw levels.[26] Noting the ionic nature of the MgO_x^+ species ($x = 1-3$), then the binding energies ought to be dominated by the difference in the ionization energies of Mg^+ and Mg^{2+}, as well as the electron affinity of O_x^-. The electron affinities for O, O_2, and O_3 are 1.461, 0.440, and 2.103 eV (141, 42, and 203 kJ mol^{-1}),[64] suggesting that the binding energy of MgO_3^+ should be the highest of the three species, as we obtain. The value reported in ref 26 is therefore concluded to be far too low. The vibrational frequencies are given in Table 1, and there do not appear to be any other values with which to compare. We also calculated the CaO_3^+ binding energy, D_0, for comparison, using the same methods as for MgO_3^+, and using the basis sets described in ref 17, obtaining a RCCSD(T) value of 354 kJ mol^{-1}, a value that is very close to the B3LYP value of 378 kJ mol^{-1} reported by Plane and co-workers.[65]

3.2. Geometries of Intermediate Complex Ions, $[X-Mg-Y]^+$. ***3.2.1. Complexes Involving Closed-Shell Ligands Only.*** Figure 1 shows the potentially important ligand-switching reactions which may occur in the MLT. As noted above, for these reactions the $[X-Mg-Y]^+$ intermediates are important and will be discussed below. There are three closed-shell ligands (N_2, CO_2, and H_2O) that are involved in these reactions, giving three intermediate complexes where the open-shell Mg^+ is solely complexed to closed-shell species. Owing to steric and electrostatic interactions it would initially be expected that the two species would approach from roughly opposite sides of the Mg^+, as seen for Ca^+,[17] but the manner in which they approach allows for a number of possible structures for each of the three intermediate complexes. We now outline a few general assumptions that were employed to reduce the number of calculations required in this body of work. The first assumption was that H_2O would approach the Mg^+ via the δ^- oxygen with the hydrogen atoms pointing away. CO_2 has the potential to approach either side-on allowing one of the δ^- oxygens to interact with the Mg^+, or side-on allowing both oxygens to interact with Mg^+. In this investigation the side-on approach has not been considered in line with our conclusions in the Ca^+ study,[17] and in line with electrostatic considerations.[39] Although N_2 is expected to bind end-on,[39] the weaker binding energy and possible effects from the other ligand in the complex suggested that in this case the preferred approach was less clear; hence both orientations were investigated. In each case the complexes were given the freedom to optimize slightly away from the higher symmetry.

The optimized geometries are shown in Figure 3a−c, and the term symbols, vibrational frequencies, and rotational constants are given in Table 3. The approach of the individual ligands in the complexes $[H_2O-Mg-N_2]^+$, $[H_2O-Mg-CO_2]^+$, and $[CO_2-Mg-N_2]^+$ is as expected with H_2O and CO_2 approaching end-on via an electronegative oxygen atom, and N_2 approaching end-on as seen in Mg^+-N_2 and in all similar work involving Ca^+,[17] K^+,[19] and Na^+.[18] However, it is the manner in which they approach with respect to one another that is surprising, as the preferred approach is from the same side of the Mg^+ cation, in contrast to the Ca^+ cases.[17] Similar geometries have been seen previously, however, by Bauschlicher and co-workers for $[Mg(CO_2)_2]^+$ [54] and $[Mg(H_2O)_2]^+$,[46] with the latter also having been observed by Watanabe et al.[43] The total energies and harmonic vibrational frequencies of the two ligands approaching from opposite sides of Mg^+ are shown in Table 3, and as can be seen these geometries give imaginary vibrational frequencies or higher total energies than for the other orientations, confirming that these structures are either saddle points or are only local minima on the potential energy surfaces, respectively. Previous work on binding with different metal cations by Bauschlicher et al.[46,54] suggests that this difference is due to a low-lying ^2D state present within calcium. These low-lying ^2D states allow sdσ hybridization which, in contrast to the sp hybridization occurring in the magnesium, reduces the charge density equally on both sides of the metal cation therefore favoring linear structures, not the bent structures observed in the case of magnesium.

Another subtlety is that there appear to be interactions between the ligands, suggesting steric repulsion (see Figure 3a−c), but clearly the electronic stabilization from sp hybridization outweighs this steric effect.

3.2.2. Geometries of $[O-Mg-X]^+$ (X = CO_2, N_2, H_2O) Intermediate Complex Ions. The oxygen atom has an open-shell ground state configuration (^3P), which made the investigation of the $[O-Mg-X]^+$ complexes more involved than that of the open-shell magnesium cation complexed to two closed-shell ligands. The reason for this is that, in addition to a number of possible complexes with different orientations for each pair of ligands, there is also the possibility that each complex could have an overall quartet or doublet spin multiplicity. The doublet state arises from the formation of a chemical bond via charge transfer from the Mg^+ to the O, leaving a formal double positive charge on the magnesium and a single negative charge on the oxygen. Our previous work on $[O-Ca-X]^+$ complexes[17] suggests that the formation of a chemical bond occurring within these complexes is likely. The calculated optimized structures for these complexes are shown in Figure 3d−f, with the vibrational frequencies and rotational constants given in Table 4. As can be seen, in contrast to the complexes discussed in section 3.2.1, the ligands all approach in an essentially end-on manner from the opposite side to the oxygen atom. The rationale for this is that Mg is formally Mg^{2+}, and hence there is not the same opportunity for sp hybridization to occur. As a consequence, the ligands approach from opposite sides on steric grounds—this is in line with the conclusions of Bauschlicher and co-workers where dicationic complexes, such as $[Mg(H_2O)_2]^{2+}$, followed this mode of bonding.[48,56] As expected, based upon our previous Ca^+ work,[17] in each case the doublet species was found to be lower in energy than the quartet species, consistent with the charge transfer from Mg^+ to O—this is evinced by both the spin and charge analyses. It can also be seen (Table 4) that the end-on approach is preferred by N_2 regardless of whether the complex in question is in its quartet or doublet state, with only slight deviations from linear approaches of this ligand.

3.2.3. Geometries of $[O_2-Mg-X]^+$ (X = CO_2, N_2, H_2O) Intermediate Complex Ions. O_2 is open shell in its ground state ($X^3\Sigma_g^-$), so considerations similar to those above are required; in addition, O_2 like N_2 could bind both end-on and side-on. Calculations on the MgO_2^+ species (vide supra) and similar studies on the $[O_2-Ca-X]^+$ intermediate complexes[17] have shown that side-on is the preferred approach of the O_2 ligand,

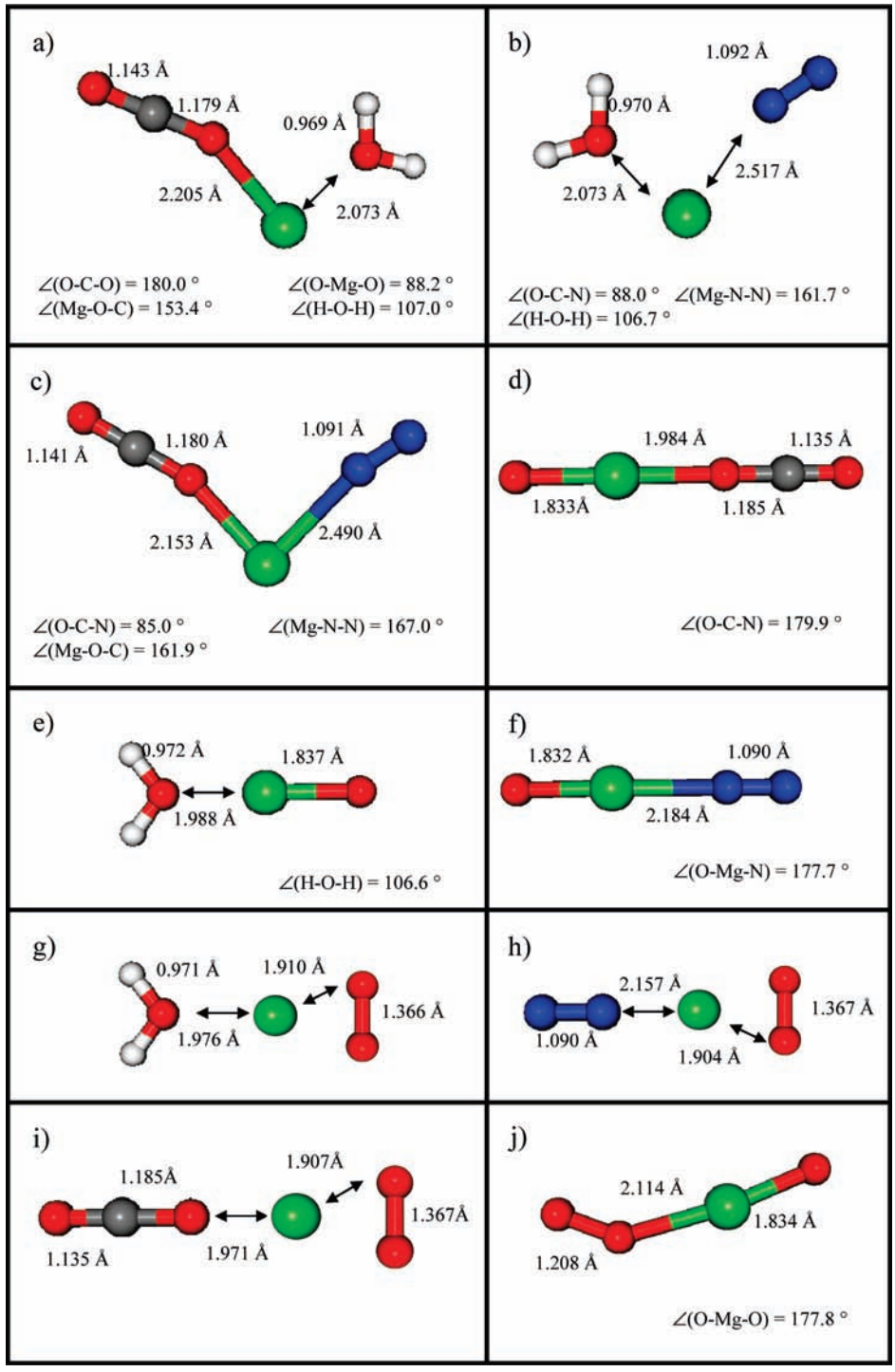

Figure 3. B3LYP/6-311+G(2d,p) optimized geometries of $[X-Mg-Y]^+$ complexes. Bond lengths in angstroms and bond angles in degrees. See text for details.

and that these complexes also exhibit charge transfer as discussed earlier, essentially giving Mg^{2+} and O_2^-; hence we expect a similar situation will arise for the $[O_2-Mg-X]^+$ complexes, with the "end-on" approach of the second ligand being favored, owing to the lack of sp hybridization on the Mg^{2+} center, as for the $[O-Mg-X]^+$ species. Both side-on and end-on approaches, for both quartet and doublet multiplicities, were investigated for completeness.

Figure 3g−i shows the optimized geometry of each $[O_2-Mg-X]^+$ global minimum, with the harmonic vibrational frequencies and rotational constants given in Table 5. As expected, in each case the lowest energy complex is achieved when O_2 approaches side-on, while the other ligand approaches end-on, resulting in a doublet, not quartet, spin state, consistent with charge transfer from the Mg^+ to O_2 occurring. The spin and charge analyses confirm that the unpaired electron is distributed equally over the two oxygen atoms. Examination of Table 5 interestingly also shows that when O_2 approaches in an end-on manner it is the quartet state that is energetically preferred in contrast to the doublet, which shows imaginary frequencies for this method of approach.

3.2.4. Geometries of $[O_2-Mg-O]^+$ Intermediate Complex Ions. Of all the complexes studied in this body of work the intermediate complex ion composed of the three open-shell O_2,

TABLE 3: Total Energies, Electronic States, and Harmonic vibrational Frequencies for X−Mg^+−Y (X, Y = CO_2, H_2O, and N_2) Complexes Optimized and Calculated at B3LYP/6-311+G(2d,p) Level of Theory[a]

X	Y	state	energy (E_h)	vibrational frequencies (cm^{-1})	rotational constants (GHz)
CO_2	N_2	$^2A'$	−498.054 913	37 (a′), 59 (a″), 74 (a′), 110 (a″), 113 (a′), 170 (a′), 237 (a′), 644 (a′), 645 (a″), 1362 (a′), 2427 (a′), 2434 (a′)	5.55, 1.22, 1.00
CO_2	N_2	$^2\Sigma^+$	−498.050 773	10i (π), 10i (π), 49 (σ), 50 (π), 50 (π), 71 (π), 71 (π), 206 (σ), 643 (π), 643 (π), 1361 (σ), 2427 (σ), 2438 (σ)	
CO_2	sN_2	$^2A_1$	−498.047 426	59i (b_2), 10 (a_1), 11 (b_1), 11 (b_2), 61 (b_2), 62 (b_1), 242 (a_1), 641 (b_2), 641 (b_1), 1364 (a_1), 2432 (a_1), 2432 (a_1)	
CO_2	H_2O	$^2A'$	−464.987 829	60 (a″), 64 (a′), 96 (a′), 154 (a″), 194 (a′), 330 (a″), 374 (a′), 512 (a′), 647 (a′), 647 (a″), 1357 (a′), 1657 (a′), 2418 (a′), 3734 (a′), 3817 (a′)	104.44, 2.13, 2.09
CO_2	H_2O	$^2A_1$	−464.979 867	57i (b_2), 52i (b_1), 26 (b_2), 26 (b_1), 86 (a_1), 305 (b_1), 329 (a_1), 457 (b_2), 652 (b_2), 652 (b_1), 1355 (a_1), 1648 (a_1), 2410 (a_1), 3706 (a_1), 3794 (b_2)	
H_2O	N_2	$^2A'$	−385.891 153	63 (a′), 99 (a″), 101(a′), 137 (a″), 154 (a′), 346 (a″), 373 (a′), 519 (a′), 1663 (a′), 2425 (a′), 3733 (a′), 3812 (a′)	12.05, 2.71, 2.21
H_2O	N_2	$^2A_1$	−385.887 152	13 (b_1), 13 (b_2), 48 (a_1), 77 (b_2), 79 (b_1), 334 (b_1), 364 (a_1), 494 (b_2), 1657 (a_1), 2438 (a_1), 3716 (a_1), 3797 (b_2)	
H_2O	sN_2	$^2A_1$	−385.884 382	54i (b_2), 45i (a_2), 12 (a_1), 24 (b_1), 24 (b_2), 347 (b_1), 382 (a_1), 509 (b_2), 1660 (a_1), 2433 (a_1), 3718 (a_1), 3795 (b_2)	

[a] Rotational constants are given for the global minima only. sN_2 denotes side-on binding; otherwise the binding is end-on.

TABLE 4: Total Energies, Electronic States, and Harmonic vibrational Frequencies for O−Mg^+−X (X = CO_2, H_2O, and N_2) Complexes Optimized and Calculated at B3LYP/6-311+G(2d,p) Level of Theory[a]

X	Y	state	energy (E_h)	vibrational frequencies (cm^{-1})	rotational constants (GHz)
N_2	O	$^2\Sigma^+$	−384.544 895	49 (π), 49 (π), 222 (π), 222 (π), 288 (σ), 830 (σ), 2453 (σ)	
N_2	O	$^4\Sigma^-$	−384.483 339	24i (π), 24i (π), 93 (σ), 104 (π), 104 (π), 148 (σ), 2441 (σ)	
N_2	O	$^2A'$	−384.578 277	46 (a′), 208 (a″), 208 (a″), 266 (a″), 742 (a′), 2452 (a′)	15 940.69, 2.12, 2.12
N_2	O	$^4A''$	−384.486 000	49 (a′), 110 (a″), 123 (a″), 136 (a″), 197 (a′), 2438 (a′)	
sN_2	O	$^2A_1$	−384.520 211	232i (b_2), 50 (b_1), 53 (b_2), 201 (a_1), 824 (a_1), 2384 (a_1)	
sN_2	O	$^4A_2$	−384.476 981	88i (b_2), 10i (b_1), 10i (b_2), 22 (a_1), 192 (a_1), 2429 (a_1)	
CO_2	O	$^2\Sigma^+$	−463.649 500	43 (π), 43 (π), 116 (π), 116 (π), 314 (σ), 631 (π),631 (π), 831 (σ), 1386 (σ), 2461 (σ)	
CO_2	O	$^4\Sigma^+$	−463.580 734	22i (π), 22i (π), 46 (π), 46 (π), 107 (σ), 198 (σ), 644 (π), 644 (π), 1360 (σ), 2424 (σ)	
CO_2	O	$^2A''$	−463.682 310	31 (a′), 84 (a″), 108 (a′), 296 (a′), 633 (a′), 633 (a″), 750 (a′), 1382 (a′), 2457 (a′)	118 080.85, 1.29, 1.29
CO_2	O	$^4A''$	−463.584 191	49 (a′), 59 (a″), 77 (a′), 181 (a′), 223 (a′), 644 (a″), 645 (a′), 1359 (a′), 2425 (a′)	
H_2O	O	$^2A''$	−351.522 120	64 (a′), 73 (a″), 413 (a′), 418 (a″), 606 (a′), 758.9(a′), 1682 (a′), 3724 (a′), 3784 (a′)	408.32, 3.91, 3.87
H_2O	O	^4A	−351.419 850	40 (a), 58 (a), 171 (a), 353 (a), 357 (a), 495 (a), 1659 (a), 3718 (a), 3798 (a)	
H_2O	O	$^2B_1$	−351.522 114	60 (b_2), 73 (b_1), 412 (a_1), 420 (b_1), 608 (b_2), 758 (a_1), 1682 (a_1), 3721 (a_1), 3781 (b_2)	
H_2O	O	$^4A_2$	−351.416 611	23i (b_2), 23i (b_1), 104 (a_1), 325 (b_1), 355 (a_1), 480 (b_2), 1654 (a_1), 3715 (a_1), 3798 (b_2)	

[a] Rotational constants are given for the global minima only. sN_2 denotes side-on binding; otherwise the binding is end-on.

O, and Mg^+ species was the most difficult, owing to the possibility of doublet, quartet, and sextet spin states in addition to a selection of different structures. Calculations were performed for O_2 approaching the strongly bound MgO^+ moiety both end-on and side-on, and for O approaching the strongly bound MgO_2^+ on both the same and opposite sides as O_2. Owing to the lowest excited singlet states of O(^{1}D) and O_2($^1\Delta_g$) being significantly higher in energy than the ground state triplets, it is expected that sextet and doublet states should not arise, except when O approaches on the same side as O_2 for which doublet and quartet states are likely; nevertheless, both were calculated for all structures for completeness.

Table 6 shows the results of these calculations, and as can be seen the lowest energy structure, as observed for Ca^+,[17] is found to be the doublet ozonide structure, the structure of which is shown in Figure 3j. For the approach of the species from opposite sides of the magnesium cation, both linear structures—where O_2 was bound end-on—and structures in which O_2 was bound side-on, giving C_{2v} symmetry, were found to be located at saddle points on the potential energy surface. Hence unconstrained searches were undertaken yielding a C_1 (^{4}A) structure, the geometry of which is shown in Figure 3j.

3.2.5. Geometries of $[Mg(X)_2]^+$ (X = CO_2, N_2, H_2O, O_2) Complex Ions. In addition to ligand-switching reactions occurring between two different ligands (reactions 7a, 7b), addition of the same ligand can initiate cluster formation (reaction 8). Thus, geometry optimizations and harmonic frequency calculations were carried out on $[X-Mg-X]^+$ complexes. End-on approaches of CO_2 and H_2O were confirmed as being saddle points, as can be seen from the imaginary frequencies in Table 7. Relaxation of the symmetry restraints allowed the complexes to approach the Mg^+ from the same side resulting in the minimum geometries that are shown in Figure 4a,b, in agreement with previous workers' conclusions,[43,46,54] with $[Mg(CO_2)_2]^+$ being of C_{2v} symmetry and $[Mg(H_2O)_2]^+$ being of C_2 symmetry; see Figure 4. A number of structures were calculated for

TABLE 5: Total Energies, Electronic States, and Harmonic Vibrational Frequencies for O_2-Mg^+-X (X = CO_2, H_2O, and N_2) Complexes Optimized and Calculated at B3LYP/6-311+G(2d,p) Level of Theory[a]

X	Y	state	energy (E_h)	vibrational frequencies (cm^{-1})	rotational constants (GHz)
CO_2	O_2	$^2\Sigma^+$	−538.860 325	66i (π), 66i (π), 10 (π), 10 (π), 37 (σ), 57 (π), 57 (π), 229 (σ), 641 (π), 641 (π), 1363 (σ), 1631 (σ), 2430 (σ)	
CO_2	O_2	$^4\Sigma^-$	−538.860 751	9 (π), 9 (π), 43 (σ), 54 (π), 54 (π), 65 (π), 65 (π),222 (σ), 642 (π), 642 (π), 1362 (σ), 1626 (σ), 2429 (σ)	
CO_2	sO_2	$^2A_2$	−538.910 676	33 (b_1), 39 (b_2), 104 (b_1), 106 (b_2), 274 (a_1), 508 (b_2), 631 (b_2), 632 (b_1), 679 (a_1), 1125 (a_1), 1386 (a_1), 2460 (a_1)	33.83, 0.99, 0.96
CO_2	sO_2	$^4B_1$	−538.859 346	39i (b_2), 11 (b_1), 13 (b_2), 27 (a_1), 60 (b_2), 60 (b_1), 236 (a_1), 641 (b_1), 641 (b_2), 1364 (a_1), 1619 (a_1), 2431 (a_1)	
H_2O	O_2	$^2A_2$	−426.697 062	53i (b_2), 52i (b_1), 23 (b_2), 25 (b_1), 37 (a_1), 342 (b_1), 375 (a_1), 503 (b_2), 1631 (a_1), 1659 (a_1), 3717 (a_1), 3796 (b_2)	
H_2O	O_2	$^4A_2$	−426.697 422	21 (b_2), 22 (b_1), 42 (a_1), 70 (b_2), 73 (b_1), 340 (b_1), 372 (a_1), 501 (b_2), 1628 (a_1), 1658 (a_1), 3717 (a_1), 3796 (b_2)	
H_2O	sO_2	$^2A_2$	−426.750 992	54 (b_2), 68 (b_1), 89 (a_2), 387 (a_1), 407 (b_1), 505 (b_2), 614 (b_2), 698 (a_1), 1126 (a_1), 1681 (a_1), 3725 (a_1), 3785 (b_2)	31.30, 2.94, 2.69
H_2O	sO_2	$^4A_2$	−426.642 722	60 (b_2), 69 (a_2), 73 (b_1), 293 (b_2), 357 (a_1), 418 (b_1), 552 (a_1), 608 (b_2), 705 (a_1), 1682 (a_1), 3723 (a_1), 3782 (b_2)	
H_2O	sO_2	^2A	−426.750 992	53 (a), 68 (a), 86 (a), 387 (a), 410 (a), 505 (a), 614 (a), 699 (a), 1127 (a), 1682 (a), 3725 (a), 3784 (a)	
H_2O	sO_2	$^4A''$	−426.699 105	35 (a′), 46 (a″), 55 (a′), 70 (a′), 133 (a″), 335 (a″), 383 (a′), 510 (a′), 1628 (a′), 1654 (a′), 3725 (a′), 3805 (a′)	
N_2	O_2	$^2\Sigma^+$	−459.761 418	94i (π), 94i (π), 7i (π), 7i (π), 46 (σ), 115 (π), 115 (π), 134 (σ), 1632 (σ), 2442 (σ)	
N_2	O_2	$^4\Sigma^-$	−459.762 151	12i (π), 12i (π), 55 (σ), 73 (π), 73 (π), 106 (π), 106 (π), 118 (σ), 1624 (σ), 2442 (σ)	
N_2	sO_2	$^2A_2$	−459.806 721	34 (b_1), 45 (b_2), 214 (b_1), 216 (b_2), 260 (a_1), 514 (b_2), 666 (a_1), 1122 (a_1), 2453 (a_1)	33.83, 1.63, 1.56
N_2	sO_2	$^4A_1$	−459.760 097	52i (b_2), 4 (b_1), 12 (b_2), 38 (a_1), 125 (b_2), 126 (b_1), 152 (a_1), 1615 (a_1), 2443 (a_1)	
N_2	O_2	$^4A''$	−459.764 048	32 (a′), 64 (a″), 68 (a′), 94 (a′), 118 (a″), 121 (a′), 163 (a′), 1620 (a′), 2441 (a′)	
sN_2	O_2	$^2A''$	−459.777 320	48 (a′), 85 (a″), 165 (a″), 170 (a′), 216 (a′), 248 (a′), 373 (a′), 1266 (a′), 2443 (a′)	
sN_2	O_2	$^4A_2$	−459.755 091	92i (b_2), 1i (b_1), 4 (b_2), 22 (a_1), 90 (b_2), 92 (b_1), 129 (a_1), 1620 (a_1), 2428 (a_1)	
N_2	O_2	$^2A''$	−459.777 320	48 (a′), 85 (a″), 164 (a″), 169 (a′), 216 (a′), 248 (a′), 374 (a′), 1266 (a′), 2444 (a′)	

[a] Rotational constants are given for the global minima only. sO_2 denotes side-on binding; otherwise the binding is end-on.

TABLE 6: Total Energies, Electronic States, and Harmonic Vibrational Frequencies for $O-Mg^+-O_2$ Complexes Optimized and Calculated at B3LYP/6-311+G(2d,p) Level of Theory[a]

X	Y	state	energy (E_h)	vibrational frequencies (cm^{-1})	rotational constants (GHz)
O	O_2	$^2\Sigma^+$	−425.345 295	62i (π), 62i (π), 53 (π), 53 (π), 272 (σ), 829 (σ), 1658 (σ)	
O	O_2	$^4\Sigma^-$	−425.379 874	73i (π), 69i (π), 37 (π), 39 (π), 245(σ), 736(σ), 1648(σ)	
O	O_2	$^6\Sigma^+$	−425.292 034	14i (π), 14 (π), 72 (σ), 89 (π), 89 (π), 166 (σ), 1620 (σ)	
O	sO_2	$^2A_2$	−425.351 319	236i (b_2), 34 (b_1), 38 (b_2), 174 (a_1), 728 (a_1), 1568 (a_1)	
O	sO_2	$^4A_1$	−425.368 037	220i (b_2), 33 (b_1), 41 (b_2), 127 (a_1), 694 (a_1), 1510 (a_1)	
O	sO_2	$^6B_2$	−425.289 275	62i (b_2), 13i (b_1), 8i (b_2), 46 (a_1), 186 (a_1), 1612 (a_1)	
O	O_2	$^2A'$	−425.380 252	36 (a′), 66 (a″), 115 (a′), 254 (a′), 736 (a′), 1625 (a′)	
O	O_2	$^4A'$	−425.380 551	48 (a′), 65 (a″), 130 (a′), 258 (a′), 730 (a′), 1610 (a′)	104.44, 2.13, 2.09
O	O_2	$^6A'$	−425.293 308	31 (a′), 69 (a′), 78 (a″), 97 (a′), 187 (a′), 1619 (a′)	
O	sO_2	$^2A'$	−425.380 243	48 (a′), 70 (a″), 122 (a′), 256 (a′), 737 (a′), 1625 (a′)	
O	sO_2	$^4A'$	−425.368 046	224i (a′), 31 (a″), 42 (a′), 135 (a′), 704 (a′), 1523 (a′)	
O	sO_2	$^6A'$	−425.292 065	12 (a′), 74 (a′), 83 (a′), 87 (a″), 166 (a′), 1621(a′)	
O_2	O	$^2A''$	−425.362 672	48 (a″), 131 (a′), 247 (a′), 528 (a′), 739 (a′), 1475 (a′)	
O_2	O	$^4A'$	−425.355 821	20 (a″), 22 (a′), 44 (a′), 53 (a′), 704 (a′), 1578 (a′)	
O_2	O	$^6A'$	−425.293 307	31 (a′), 67 (a′), 76 (a″), 96 (a′), 187 (a′), 1619 (a′)	
O	O_2	$^2B_1$	−425.403 527	261 (b_1), 446 (b_2), 476 (a_1), 766 (a_1), 872 (b_2), 1066 (a_1)	
O	O_2	$^4B_1$	−425.295 366	28i (b_2), 42 (a_1), 61 (b_1), 521 (b_2), 654 (a_1), 1110 (a_1)	
O	O_2	$^6A_1$	−425.276 391	95i (b_2), 12i (b_1), 15 (a_1), 19 (b_2), 81 (a_1), 1601 (a_1)	

[a] Rotational constants are given for the global minima only. sO_2 denotes side-on binding; otherwise the binding is end-on.

$[Mg(N_2)_2]^+$ and again a bent structure was located at the global minimum, giving a C_{2v} structure (Figure 4c). These "bent" structures are in contrast to the linear structures observed in the corresponding $[Ca(X)_2]^+$ complexes,[17] and as mentioned above are thought to be due to low-lying ^2D states in the calcium allowing sdσ hybridization,[46,54] which reduces charge density equally on both sides of the metal cation, favoring the linear structure. Another way of viewing this is that in $[Mg(X)_2]^+$ sp hybridization occurs on complexation of the first H_2O creating a region of high electron density on the side opposite the first water, explaining why the second water approaches from the same side.

TABLE 7: Total Energies, Electronic States, and Harmonic vibrational Frequencies for X−Mg^+−X (X = O_2, CO_2, H_2O, and N_2) Complexes Optimized and Calculated at B3LYP/6-311+G(2d,p) Level of Theory[a]

complex	state	energy (E_h)	vibrational frequencies (cm^{-1})	rotational constants (GHz)
$CO_2-Mg^+-CO_2$	$^2A_1$	−577.151 644	30 (a_1), 49 (b_1), 57 (a_2), 58 (a_1), 89 (a_1), 212 (b_2), 233 (a_1), 643 (b_2), 645 (a_1), 645 (a_2), 646 (b_1), 1361 (b_2), 1363 (a_1), 2416 (b_2), 2433 (a_1)	5.19, 0.78, 0.68
$CO_2-Mg^+-CO_2$	$^2\Sigma_g^+$	−577.144 928	45i (π_u), 45i (π_u), 19 (π_u), 19 (π_u), 31 (π_g), 31 (π_g), 96 (σ_g), 151 (σ_u), 647 (π_g), 647 (π_g) 648 (π_u), 647.6 (π_u), 1356 (σ_u), 1357 (σ_g), 2411 (σ_u), 2419 (σ_g)	
$H_2O-Mg^+-H_2O$	^2A	−352.822 190	67 (a), 87 (a), 205 (a), 335 (a), 342 (a), 356 (a), 364 (a), 472 (a), 523 (a), 1652 (a), 1657 (a), 3724 (a), 3725 (a), 3808 (a), 3808 (a)	15.26, 5.50, 4.10
$H_2O-Mg^+-H_2O$	^2A_g	−352.813 540	84i (b_{2u}), 68i (b_{3u}), 52i (a_u), 234 (a_g), 276 (b_{2g}), 281 (b_{3u}), 370 (b_{1u}), 395 (b_{2u}), 442 (b_{23g}), 1637.4 (b_{1gu}), 1638 (a_g), 3693 (b_{1u}), 3693 (a_g), 3786 (b_{3g}), 3786 (b_{2u})	
$N_2-Mg^+-N_2$	$^2A_1$	−418.957 375	50 (a_1), 114 (b_1), 116 (a_1), 123 (b_2), 128 (a_2), 155 (b_2), 213 (a_1), 2433 (a_1), 2435 (b_2)	5.88, 2.08, 1.54
$N_2-Mg^+-N_2$	$^2\Sigma_g^+$	−418.953 181	21i (π), 21i (π), 81 (σ), 83 (σ), 93 (π), 93 (π), 94 (π), 94 (π), 2440 (σ), 2441 (σ)	
$sN_2-Mg^+-N_2$	$^2A_1$	−418.947 964	77i (b_2), 11 (b_2), 11 (b_1), 18 (a_1), 129 (b_2), 129 (b_1), 160 (a_1), 2430 (a_1), 2443 (a_1)	
$sN_2-Mg^+-sN_2$	^2A_g	−418.937 588	125i (b_{2u}), 121i (b_{3g}), 12i (b_{3u}), 6i (a_u), 11 (b_{2u}), 35 (a_g), 51 (b_{1u}), 2422 (b_{1u}), 2422 (a_g)	
$sO_2-Mg^+-O_2$	$^2B_2$	−500.549 672	183i (b_1), 112i (b_2), 5i (b_1), 3 (b_2), 27 (a_1), 83 (b_2), 113 (a_1), 1620 (a_1), 1621 (a_1)	
$sO_2-Mg^+-sO_2$	^2A_g	−500.452 940	161i (b_{2u}), 142i (b_{3g}), 18i (b_{3u}), 9 (a_u), 24 (b_{2u}), 85 (a_g), 119 (b_{1u}), 1595 (b_{1u}), 1596 (a_g)	
$O_2-Mg^+-O_2$	$^4A'$	−500.608 190	22 (a″), 40 (a′), 55 (a″), 108 (a′), 244 (a′), 505 (a′), 594 (a′), 1098 (a′), 1573 (a′)	29.60, 1.58, 1.50
$O_2-Mg^+-O_2$	$^4\Sigma_g^-$	−500.567 983	132i (π), 132i (π), 130i (π), 130i (π), 11i (π), 11i (π), 60 (σ), 60 (σ), 1629 (σ), 1629 (σ)	
$sO_2-Mg^+-O_2$	$^4A_1$	−500.607 931	65i (b_1), 52i (b_1), 36 (b_1), 50 (b_2), 241 (a_1), 504 (b_2), 594 (a_1), 1102 (a_1), 1595 (a_1)	
$sO_2-Mg^+-sO_2$	^4A_g	−500.561 097	155i (b_{2u}), 148i (b_{3g}), 11i (b_{3u}), 16 (b_{2u}), 18 (a_u), 34 (a_g), 54 (b_{1u}), 1615 (b_{1u}), 1616 (a_g)	
$O_2-Mg^+-O_2$	$^6A_1$	−500.571 144	22 (a_1), 56 (b_2), 63 (a_2), 68 (b_1), 69 (a_1), 93 (b_2), 119 (a_1), 1620 (b_2), 1621 (a_1)	
$O_2-Mg^+-O_2$	$^6\Sigma_g^+$	−500.570 254	11i (π), 11i (π), 70 (σ), 71 (π), 71 (π), 81 (σ), 82 (π), 82 (π), 1620 (σ), 1621 (σ)	
$sO_2-Mg^+-O_2$	$^6A_1$	−500.500 029	85i (b_2), 70i (b_1), 43 (b_1), 60 (b_2), 229 (a_1), 284 (b_2), 504 (a_1), 688 (a_1), 1656 (a_1)	
$sO_2-Mg^+-sO_2$	^6A_g	−500.563 112	88i (b_{2u}), 79i (b_{3g}), 18i (b_{3u}), 22 (b_{2u}), 23 (a_u), 51 (a_g), 79 (b_{1u}), 1604 (b_{1u}), 1605 (a_g)	

[a] Rotational constants are given for the global minima only. sO_2 and sN_2 denote side-on binding; otherwise the binding is end-on.

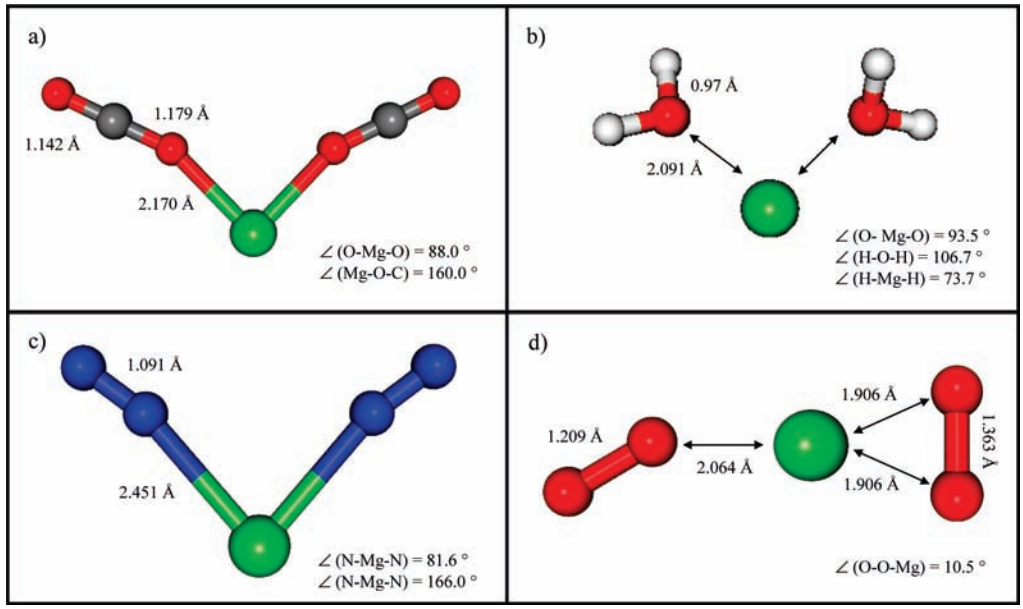

Figure 4. B3LYP/6-311+G(2d,p) optimized geometries of $[MgX_2]^+$ complexes. Bond lengths in angstroms and bond angles in degrees. See text for details.

Calculations examining the $[Mg(O_2)_2]^+$ complex, like the calculations described above on $[O-Mg-O_2]^+$, were carried out on a number of structures which in turn were calculated with doublet, quartet, and sextet multiplicities. As can be seen

TABLE 8: RCCSD(T) Total Energies

species	total energy (E_h)
CO_2	−188.389 569
H_2O	−76.363 532
O	−74.994 931
O_2	−150.177 984
N_2	−109.407 028
Mg^+	−199.675 055
Mg^+-CO_2	−388.090 767
Mg^+-H_2O	−276.090 811
Mg^+-N_2	−309.094 512
Mg^+-O	−274.750 982
Mg^+-sO_2	−349.888 824
$H_2O-Mg^+-CO_2$	−464.500 076
$N_2-Mg^+-CO_2$	−497.507 368
$N_2-Mg^+-H_2O$	−385.506 604
$N_2-Mg^+-O_2$	−459.334 294
N_2-Mg^+-O	−384.197 470
$O_2-Mg^+-H_2O$	−426.337 227
$O-Mg^+-CO_2$	−463.197 985
$O-Mg^+-H_2O$	−351.199 964
$O_2-Mg^+-CO_2$	−538.334 632
O_2-Mg^+-O	−424.958 359
$N_2-Mg^+-N_2$	−418.513 185
$O_2-Mg^+-O_2$	−500.094 642
$CO_2-Mg^+-CO_2$	*a*
$H_2O-Mg^+-H_2O$	−352.497 574

[a] Exceeded resources.

TABLE 9: Binding Energies, D_0 (D_e), for $X-Mg^+-Y$ Complexes (kJ mol^{-1})

	removal of X		removal of Y	
species	B3LYP	RCCSD(T)	B3LYP	RCCSD(T)
$H_2O-Mg^+-CO_2$	108 (116)	112 (120)	39 (43)	48 (52)
$N_2-Mg^+-CO_2$	16 (20)	22 (25)	50 (52)	59 (61)
$N_2-Mg^+-H_2O$	14 (18)	20.0 (23)	117 (124)	120 (128)
$N_2-Mg^+-O_2$	96 (101)	96 (101)	119 (125)	156 (162)
N_2-Mg^+-O	86 (91)	91 (96)	266 (272)	277 (284)
$O_2-Mg^+-H_2O$	139 (145)	173 (180)	218 (228)	214 (223)
$O-Mg^+-CO_2$	278 (284)	289 (295)	132 (135)	140 (143)
$O-Mg^+-H_2O$	285 (292)	293 (300)	207 (216)	208 (217)
$O_2-Mg^+-CO_2$	131 (136)	167 (173)	142 (145)	144 (148)
O_2-Mg^+-O	124 (128)	66 (69)	282 (285)	193 (196)
$N_2-Mg^+-N_2$		28 (31)	22 (25)	
$O_2-Mg^+-O_2$		71 (73)	74 (75)	
$CO_2-Mg^+-CO_2$		*a*	42 (45)	
$H_2O-Mg^+-H_2O$		105 (114)	101 (110)	

[a] Exceeded resources.

in Table 7, the global minimum was the $^4A'$ complex shown in Figure 4d. Similarities can be seen between this structure and the one calculated for $O-Mg^+-O_2$ in which the two ligands approached from different sides, as in both cases the approaching O_2 ligand is slightly bent away from the central axis.

3.2.6. $[X-Mg-Y]^+$ and $[X-Mg-X]^+$ RCCSD(T) Calculations. Accurate total energies are required for elucidating possible reaction pathways, as well as for applying statistical theories such as RRKM to obtain rate coefficients for reactions occurring in the upper atmosphere (Figure 1).[17−20] Hence, single-point RCCSD(T) calculations were performed at the B3LYP/6-311+G(2d,p) optimized geometries. In Table 8, the RCCSD(T)/aug-cc-pVQZ energies calculated are presented from which the binding energies in Table 9 are derived. In addition, in Table 9, the B3LYP binding energies are shown. The general behavior of the B3LYP versus RCCSD(T) binding energies is very similar to that observed in Table 2 for removal of the corresponding ligand.

Previous theoretical binding energies are only available for $[Mg(H_2O)_2]^+$ and $[Mg(CO_2)_2]^+$; in the case of $[Mg(H_2O)_2]^+$ our RCCSD(T) D_e value of 113.5 kJ mol^{-1} compares well to that of 109.6 kJ mol^{-1} obtained using the MCPF approach with a fairly large basis set,[45] and 112.1 kJ mol^{-1} using the MP4 approach.[43] It may also be seen that the B3LYP value obtained herein is in excellent agreement with those obtained at the higher levels of theory. For $[Mg(CO_2)_2]^+$, our B3LYP D_e value of 44.6 kJ mol^{-1} is in excellent agreement with the value of 46 kJ mol^{-1} obtained by Sodupe et al.[54] at the MCPF level of theory. We were unable to obtain a RCCSD(T) value for this ion as the calculation exceeded our available resources.

Both these papers are also in agreement with our observation that the removal of a water molecule from $[Mg(H_2O)_2]^+$ requires less energy than from Mg^+-H_2O, opposite to the finding for $[Ca(H_2O)_2]^+$,[17] but in line with the rest of the results on Ca^+, and those in the current study, that the removal of a ligand from $[Y-Mg-X]^+$ (where Y and X = H_2O, CO_2, and N_2) is smaller than the removal of the same ligand from Mg^+-X (where X = H_2O, CO_2, and N_2). However, with $[Y-Mg-X]^+$ (where Y = O or O_2 and X = H_2O, CO_2, and N_2) the energy for removal of the closed-shell ligand is significantly higher than that from Mg^+-X (where X = H_2O, CO_2, and N_2), in line with the formal Mg^{2+} in these complexes.

4. Conclusions

We have obtained optimized geometries and vibrational frequencies for a range of Mg^+-containing complexes which are thought to be of importance in the chemistry of magnesium in the MLT region of the Earth's atmosphere. For the Mg^+-L complexes, there was generally agreement with previous experimental and theoretical results, where available. There were, however, discrepancies with some values, in particular for Mg^+-O_3. The level of theory, the expected trend for MgO^+, MgO_2^+, and MgO_3^+, and the general agreement with experiment and the previous highest levels of calculations, suggests that the previously reported[26] low value for $D_0[Mg^+-O_3]$ is in error, as is a very low value for $D_0[Mg^+-O_2]$.[57]

We have also calculated energies for removal of each ligand from $[X-Mg-Y]^+$ complexes, after having first established the global minima. We find that for the species which have X = O or O_2 as a ligand, the binding energy of the second ligand, Y, is greater than in the Mg^+-Y complex, owing to the higher formal charge on the magnesium atom.

In line with previous work, we find the diligated complexes, where the ligand is H_2O, CO_2, or N_2, prefer to have the two ligands approaching from the same side, in contrast to the case for the calcium-containing complexes.[17] This is in line with results obtained for $[MgX_2]^+$ and $[CaX_2]^+$ complexes, where spσ hybridization in the magnesium species leads to the same side being preferred for the two ligands, whereas sdσ hybridization leads to different sides being preferred in the case of calcium. Interestingly, for the corresponding dications $[MgX_2]^{2+}$ approach from different sides is favored (as the hybridization cannot occur),[46,54] and this is consistent with the results we find for the $[O-Mg-Y]^+$ and $[O_2-Mg-Y]^+$ complexes, where the magnesium is formally doubly charged.

The results of the calculations reported here will now be used in modeling laboratory studies of many of these reactions, for later inclusion in a new atmospheric model of magnesium.[59]

Acknowledgment. The authors are grateful for the provision of computer time from the EPSRC under the auspices of the NSCCS. R.J.P. is grateful to the EPSRC for a studentship.

J.M.C.P. thanks the European Office of Aerospace Research and Development (Award No. FA8655-09-1-3015) for support.

References and Notes

(1) Plane, J. M. C. *Chem. Rev.* **2003**, *103*, 4963.
(2) Brown, T. L. *Chem. Rev.* **1973**, *73*, 645.
(3) Plane, J. M. C. *Int. Rev. Phys. Chem.* **1991**, *10*, 55.
(4) *Meteors in the Earth's Atmosphere*; Murad, E., Williams, I. W., Eds.; Cambridge University Press, Cambridge, 2002.
(5) Johnson, K. S. *Global Biogeochem. Cycles* **2001**, *15*, 61.
(6) Plane, J. M. C.; Helmer, M. *Faraday Discuss.* **1995**, *100*, 411.
(7) Molina-Cuberos, G. J.; Lammer, H.; Stumptner, W.; Schwingenshuh, K.; Rucker, H. O.; López-Moreno, J. J.; Rodrigo, R.; Tokano, T. *Planet. Space Sci.* **2001**, *49*, 143.
(8) Vondrak, T.; Plane, J. M. C.; Broadley, S.; Janches, D. *Atmos. Chem. Phys.* **2008**, *8*, 7015.
(9) McNeil, W. J.; Lai, S. T.; Murad, E. *J. Geophys. Res.* **1998**, *103*, 10899.
(10) Tepley, C. A.; Raizada, S.; Zhou, Q. H.; Friedman, J. S. *Geophys. Res. Lett.* **2003**, *30*, Article No, 1009.
(11) Clemesha, B. R. *J. Atmos. Terr. Phys.* **1995**, *57*, 725.
(12) Von Zahn, U.; Hansen, G.; Kurzawa, H. *Nature* **1988**, *331*, 594.
(13) Kane, T. J.; Gardner, C. S.; Zhou, Q.; Mathews, J. D.; Tepley, C. A. *J. Atmos. Terr. Phys.* **1993**, *55*, 499.
(14) Collins, S. C.; Plane, J. M. C.; Kelley, M. C.; Wright, T. G.; Soldan, P.; Kane, T. J.; Gerrard, A. J.; Grime, B. W.; Rollason, R. J.; Friedman, J. S.; Gonzalez, S. A.; Zhou, Q. H.; Sulzer, M. P.; Tepley, C. A. *J. Atmos. Sol.-Terr. Phys.* **2002**, *64*, 845.
(15) Bautista, M. A.; Romano, P.; Pradham, A. K. *Astrophys. J., Suppl. Ser.* **1998**, *118*, 259.
(16) Witt, G. The nature of noctilucent clouds. *Space Res.* **1969**, *9*, 157–169.
(17) Plowright, R. J.; Wright, T. G.; Plane, J. M. C. *J. Phys. Chem. A* **2008**, *112*, 6550.
(18) Daire, S. E.; Plane, J. M. C.; Gamblin, S. D.; Soldán, P.; Lee, E. P. F.; Wright, T. G. *J. Atmos. Sol.-Terr. Phys.* **2002**, *64*, 863.
(19) Plane, J. M. C.; Plowright, R. J.; Wright, T. G. *J. Phys. Chem. A* **2006**, *110*, 3093.
(20) Broadley, S.; Vondrak, T.; Wright, T. G.; Plane, J. M. C. *Phys. Chem. Chem. Phys.* **2008**, *10*, 5287.
(21) Swider, W. *Planet. Space Sci.* **1984**, *32*, 307.
(22) Kopp, E.; Eberhardt, P.; Hermann, U.; Bjorn, L. G. *J. Geophys. Res.* **1985**, *90*, 13041.
(23) von Zahn, U.; Goldberg, R. A.; Stegman, J.; Witt, G. *Planet. Space Sci.* **1989**, *37*, 657.
(24) Anderson, J. G.; Barth, C. A. *J. Geophys. Res.* **1971**, *76*, 3723.
(25) Gerard, J.-C.; Monfils, A. *J. Geophys. Res.,* **1974**, *79*, 2544.
(26) Petrie, S. *Environ. Chem.* **2005**, *2*, 308.
(27) Petrie, S.; Dunbar, R. C. Astrochemistry: From Laboratory Studies to Astronomical Observations. *AIP Conf. Proc.* **2006**, *855*, 272.
(28) Frizenwallner, J.; Kopp, E. *Adv. Space Res.* **1998**, *21*, 859.
(29) Petrie, S.; Dunbar, R. C. *J. Phys. Chem. A* **2000**, *104*, 4480.
(30) Petrie, S. *Environ. Chem.* **2005**, *2*, 25.
(31) Ferguson, E. E.; Rowe, B. R.; Fahey, D. W.; Fehsenfeld, F. C. *Planet. Space Sci.* **1981**, *29*, 479.
(32) Murray, B. J.; Plane, J. M. C. *Atmos. Chem. Phys.* **2005**, *5*, 1027–1038.
(33) Frisch, M. J.; Trucks, G. W.; Schlegel, H. B.; Scuseria, G. E.; Robb, M. A.; Cheeseman, J. R.; Montgomery, J. A., Jr.; Vreven, T.; Kudin, K. N.; Burant, J. C.; Millam, J. M.; Iyengar, S. S.; Tomasi, J.; Barone, V.; Mennucci, B.; Cossi, M.; Scalmani, G.; Rega, N.; Petersson, G. A.; Nakatsuji, H.; Hada, M.; Ehara, M.; Toyota, K.; Fukuda, R.; Hasegawa, J.; Ishida, M.; Nakajima, T.; Honda, Y.; Kitao, O.; Nakai, H.; Klene, M.; Li, X.; Knox, J. E.; Hratchian, H. P.; Cross, J. B.; Bakken, V.; Adamo, C.; Jaramillo, J.; Gomperts, R.; Stratmann, R. E.; Yazyev, O.; Austin, A. J.; Cammi, R.; Pomelli, C.; Ochterski, J. W.; Ayala, P. Y.; Morokuma, K.; Voth, G. A.; Salvador, P.; Dannenberg, J. J.; Zakrzewski, V. G.; Dapprich, S.; Daniels, A. D.; Strain, M. C.; Farkas, O.; Malick, D. K.; Rabuck, A. D.; Raghavachari, K.; Foresman, J. B.; Ortiz, J. V.; Cui, Q.; Baboul, A. G.; Clifford, S.; Cioslowski, J.; Stefanov, B. B.; Liu, G.; Liashenko, A.; Piskorz, P.; Komaromi, I.; Martin, R. L.; Fox, D. J.; Keith, T.; Al-Laham, M. A.; Peng, C. Y.; Nanayakkara, A.; Challacombe, M.; Gill, P. M. W.; Johnson, B.; Chen, W.; Wong, M. W.; Gonzalez, C.; Pople, J. A. *Gaussian 03*, Revision C.02; Gaussian, Inc.: Wallingford, CT, 2004.
(34) Werner, H.-J.; Knowles, P. J.; Lindh, R.; Manby, F. R.; Schütz, M.; Celani, P.; Korona, T.; Mitrushenkov, A.; Rauhut, G.; Adler, T. B.; Amos, R. D.; Bernhardsson, A.; Berning, A.; Cooper, D. L.; Deegan, M. J. O.; Dobbyn, A. J.; Eckert, F.; Goll, E.; Hampel, C.; Hetzer, G.; Hrenar, T.; Knizia, G.; Köppl, C.; Liu, Y.; Lloyd, A. W.; Mata, R. A.; May, A. J.; McNicholas, S. J.; Meyer, W.; Mura, M. E.; Nicklass, A.; Palmieri, P.; Pflüger, K.; Pitzer, R.; Reiher, M.; Schumann, U.; Stoll, H.; Stone, A. J.; Tarroni, R.; Thorsteinsson, T.; Wang, M.; Wolf, A. *MOLPRO, version 2008.1, a package of ab initio programs*; see http://www.molpro.net.
(35) Ochterski, J. W.; Petersson, G. A.; Montgomery, J. A., Jr. *J. Chem. Phys.* **1996**, *104*, 2598.
(36) Operti, L.; Tews, E. C.; MacMahon, T. J.; Freiser, B. S. *J. Am. Chem. Soc.* **1989**, *111*, 9152.
(37) Yeh, C. S.; Willey, K. F.; Robbins, D. L.; Pilgrim, J. S.; Duncan, M. A. *Chem. Phys. Lett.* **1992**, *196*, 233.
(38) Willey, K. F.; Yeh, C. S.; Robbins, D. L.; Pilgrim, J. S.; Duncan, M. A. *J. Chem. Phys.* **1992**, *97*, 8886.
(39) Duncan, M. A. *Annu. Rev. Phys. Chem.* **1997**, *48*, 69.
(40) Misaizu, F.; Sanekata, M.; Tsukamoto, K.; Fuke, K.; Iwata, S. *J. Phys. Chem.* **1992**, *96*, 8259.
(41) Fuke, K.; Misaizu, F.; Sanekata, M.; Tsukamoto, K.; Iwata, S. *Z. Phys. D* **1993**, *26*, S180.
(42) Misaizu, F.; Sanekata, M.; Fuke, K.; Iwata, S. *J. Chem. Phys.* **1994**, *100*, 1161.
(43) Watanabe, H.; Iwata, S.; Hashimoto, K.; Misaizu, F.; Fuke, K. *J. Am. Chem. Soc.* **1995**, *117*, 755.
(44) Watanabe, H.; Iwata, S. *J. Chem. Phys.* **1998**, *108*, 10078.
(45) Bauschlicher, C. W., Jr.; Partridge, H. *J. Phys. Chem.* **1991**, *95*, 3946.
(46) Bauschlicher, C. W.; Sodupe, M.; Partridge, H. *J. Chem. Phys.* **1992**, *96* (6), 4453.
(47) Sodupe, M.; Bauschlicher, C. W., Jr. *Chem. Phys. Lett.* **1992**, *195*, 494.
(48) Andersen, A.; Muntean, F.; Walter, D.; Rue, C.; Armentrout, P. B. *J. Phys. Chem. A* **2000**, *104*, 692.
(49) Dunbar, R. C.; Petrie, S. *J. Phys. Chem. A* **2005**, *109*, 1411.
(50) Tachikawa, H.; Yoshida, H. *J. Mol. Struct. (THEOCHEM)* **1996**, *363*, 263.
(51) Maitre, P.; Bauschlicher, C. W.; Partridge, H. *Chem. Phys. Lett.* **1994**, *225*, 467.
(52) Robbins, D. L.; Brock, L. R.; Pilgrim, J. S.; Duncan, M. A. *J.Chem. Phys* **1995**, *102*, 1481.
(53) Willey, K. F.; Yeh, C. S.; Robbins, D. L.; Duncan, M. A. *Chem. Phys. Lett.* **1992**, *192*, 179.
(54) Sodupe, M.; Bauschlicher, C. W.; Partridge, H. *Chem. Phys. Lett.* **1992**, *192*, 185.
(55) Bauschlicher, C. W.; Langhoff, S. R.; Partridge, H. *J. Chem. Phys.* **1994**, *101* (3), 2644.
(56) Partridge, H.; Langhoff, S. R.; Bauschlicher, C. W., Jr. *J. Chem. Phys.* **1986**, *84*, 4486.
(57) Jursic, B. S. *J. Mol. Struct. (THEOCHEM)* **2000**, *530*, 59.
(58) Kappes, M. M.; Staley, R. H. *J. Phys. Chem.* **1981**, *85*, 942.
(59) Whicker, C. L.; Gomez Martin, J. C.; Wright, T. G.; Plane, J. M. C., to be submitted.
(60) Rowe, B. R.; Fahey, D. W.; Ferguson, E. E.; Fehsenfeld, F. C. *J. Chem. Phys.* **1981**, *75*, 3325.
(61) Dalleska, N. F.; Armentrout, P. B. *Int. J. Mass Spectrom. Ion Processes* **1994**, *134* (2−3), 203.
(62) Sodupe, M.; Bauschlicher, C. W. *Chem. Phys. Lett.* **1993**, *203*, 215.
(63) Chen, J.; Wong, T. H.; Kleiber, P. D. *J. Chem. Phys.* **1998**, *109* (19), 8311.
(64) Lias, S. G.; Bartmess, J. E.; Liebman, J. F.; Holmes, J. L.; Levin, R. D.; Mallard, W. G. Gas-Phase Ion and Neutral Thermochemistry. *J. Phys. Chem. Ref. Data* **1988**, *17* (Suppl. 1).
(65) Broadley, S. L.; Vondrak, T.; Plane, J. M. C. *Phys. Chem. Chem. Phys.* **2007**, *9*, 4357.

JP905642H